

# Four-wave Mixing-based Wavelength Conversion and Parametric Amplification in Submicron Silicon Core Fibers

Dong Wu, Li Shen, Haonan Ren, Meng Huang, Cosimo Lacava, Joseph Campling, Shiyu Sun, Thomas W. Hawkins, Ursula J. Gibson, Periklis Petropoulos, John Ballato, and Anna C. Peacock

**Abstract**—Silicon core fibers represent a versatile platform for all-fiber integrated nonlinear optical applications. This paper describes the state of the art in four-wave mixing-based parametric amplification and wavelength conversion in silicon fibers that have been tapered to improve the material quality and engineer the dispersion profile. Fibers with submicron core dimensions have been fabricated and used to demonstrate high gain parametric amplification in the C-Band and broadband wavelength conversion extending out to the S- and L-bands. The potential to use these fibers for all-optical signal processing of 20 Gbit/s data signals has also been demonstrated, with a robust all-fiber coupling scheme presented to improve the efficiency and practicality of these devices. These results highlight the potential of silicon core fibers for use in nonlinear signal processing within future telecommunication systems.

**Index Terms**—Fiber optics, nonlinear optics, four-wave mixing, silicon photonics.

## I. INTRODUCTION

FOUR-wave mixing (FWM) is one of the most widely studied nonlinear effects for all-optical signal processing as it can be exploited for various useful functions such as signal amplification, regeneration, wavelength conversion, and demultiplexing. Over the past two decades, high-performance FWM has been investigated both in highly nonlinear fibers

(HNLF) [1]–[3] and integrated waveguides [4]–[10] across the telecom wavelength bands. When deciding which platform to use, the relative advantages and drawbacks of each one must be carefully considered. For example, fibers tend to offer significantly lower transmission losses, but, typically, the glassy core has a much lower nonlinearity than the semiconductors used in planar integrated circuits, and so require the use of much longer lengths (tens of meters vs millimeters) and higher operating powers [1], [11]. Moreover, while HNLFs can be readily integrated with other fiber systems, planar platforms such as silicon-on-insulator (SOI) waveguides offer a route towards small footprint photonic circuits on chip [12], [13]. Recently, a new platform has emerged in which crystalline silicon materials are embedded into the cores of optical fibers. These silicon core fibers (SCFs) combine several benefits of the fiber geometry with those of the highly nonlinear semiconductor waveguide materials, and are already showing great promise for various nonlinear applications across a broad wavelength range [14], [16]–[19]. It is worth noting that the strong nonlinear absorption in crystalline silicon has meant that it is not always the first choice for signal processing in the telecoms band, and many researchers have moved to consider alternative materials that have suppressed nonlinear losses such as amorphous silicon [6], silicon nitride [9], or AlGaAs [10], but which can be more complicated to fabricate. However, through careful design and processing of the SCFs to engineer the dispersion and achieve low transmission losses, this new platform has allowed for efficient nonlinear processing within the crystalline silicon core at modest input powers within this important wavelength region [18].

A key benefit of the SCF platform is that the fibers can be fabricated using the molten core drawing (MCD) technique, which is fast and efficient, and produces fibers that are readily compatible with standard fiber post-processing procedures [20]. In particular, although the SCFs typically produced via the MCD method have core sizes of  $\sim 10 \mu\text{m}$ , by using a conventional fiber tapering post-processing procedure it has been possible to reduce the core sizes down to the submicrometer dimensions required for efficient nonlinear processing [14]. Moreover, as the silicon undergoes complete melting during the tapering process, by controlling the cooling dynamics of the recrystallization it is also possible to improve the material quality of the core to obtain losses that are comparable to, if not lower than, their planar nanowire waveguide counterparts [15], [21]. As well as providing a means to rapidly produce

Manuscript received XX XX, 2020; revised XX XX, 2020; accepted XX XX, 2020. Date of publication XX XX, 2020; date of current version XX XX, 2020. This work was supported by the following research funds: Engineering and Physical Sciences Research Council (EPSRC) (EP/P000940/1, EP/N013247/1, EP/S002871/1); National Natural Science Foundation of China (NSFC) (61705072); the Norwegian Research Council (262232); the J. E. Serrine Foundation. The data for this work are accessible through the University of Southampton Institutional Research Repository (doi.org/10.5258/SOTON/Dxxxx). (Corresponding author: Li Shen)

D. Wu, H. Ren, M. Huang, J. Campling, S. Sun, P. Petropoulos, and A. C. Peacock are with the Optoelectronics Research Centre, University of Southampton, Southampton SO17 1BJ, U.K. (e-mail: D.Wu@soton.ac.uk; hr2d19@soton.ac.uk; M.Huang@soton.ac.uk; J.Campling@soton.ac.uk; S.Sun@soton.ac.uk; pp@orc.soton.ac.uk; acp@orc.soton.ac.uk).

L. Shen is with Wuhan National Laboratory for Optoelectronics, School of Optical and Electronic Information, Huazhong University of Science and Technology, Wuhan 430074, Hubei, China. (e-mail: lishen@hust.edu.cn).

C. Lacava was with the University of Southampton. He is currently with Università di Pavia, Via Ferrata, 5A, 27100 Pavia, Italy. (e-mail: cosimo.lacava@unipv.it).

T. W. Hawkins, and J. Ballato are with the Center for Optical Materials Science and Engineering Technologies and the Department of Materials Science and Engineering, Clemson University, Clemson, SC 29634, USA. (e-mail: hawkin2@clemson.edu; jballat@clemson.edu).

U. J. Gibson is with Department of Physics and Porelabs, Norwegian University of Science and Technology, N-7491 Trondheim, Norway. She is also at Department of Applied Physics, KTH Royal Institute of Technology, Stockholm 10044, Sweden. (e-mail: ursula.gibson@ntnu.no).

low loss, small core SCFs, tapering also allows for precise tailoring of the fiber dimensions along the length, which is important for improving coupling conditions and dispersion engineering for nonlinear processes that require phase matching [22]. Initial work in tapered SCFs with few-micrometer core sizes produced various nonlinear demonstrations, including multiphoton absorption and self-phase modulation (SPM) in the telecoms band [14], as well as supercontinuum generation using mid-infrared pump wavelengths [19]. More recently, SCFs with submicron core dimensions have been utilized for optical parametric amplification (OPA) with a maximum gain of  $\sim 9$  dB, when pumped by a pulsed fiber laser operating at telecoms wavelengths [18]. Thus, these submicron core size SCFs are showing great promise for all-optical signal processing applications in the telecom band, with performances comparable to their planar waveguide counterparts, but with the benefit of potential integration with fiber pump sources.

In this paper, we review recent work on FWM nonlinear signal processing in submicron SCFs including wavelength conversion and OPA, with a view to benchmarking their performance for signal processing applications across the extended telecommunications band. A brief overview of the fabrication procedures used to make the submicron SCFs using conventional processing techniques is first provided. Then, a theoretical model is presented to better understand the phase matching conditions required for efficient, broadband FWM conversion for comparison with the experimental results. Wavelength conversion over a bandwidth of more than 260 nm has been achieved, with a net off-fiber gain of  $\sim 2$  dB being realized in the C-band, in good agreement with the predictions. By exploiting the large FWM gain bandwidth of the SCFs, we present the first demonstrations of wavelength conversion of 20 Gb/s quadrature phase-shift keying (QPSK) signals across the S, C and L-bands. Finally, some perspectives are provided on the opportunities of using tapered SCFs for all fiber nonlinear systems.

## II. SILICON CORE FIBER FABRICATION AND TAPERING METHOD

Since the first demonstration of a SCF in 2006, there have been two main fabrication methods employed in their production; the high pressure chemical vapor deposition (HPCVD)

technique [23] and the MCD method [20]. In the HPCVD method, SCFs are fabricated by depositing silicon directly into the central pore of silica capillaries that are usually limited to a few centimeters in length due to the slow silicon deposition rate. In contrast, the MCD method uses a modified form of the conventional glass fiber drawing tower approach, and thus can rapidly produce SCFs of kilometers in length. Moreover, owing to the longer lengths, the MCD SCFs are compatible with standard tapering treatments, which can be applied to tailor the core dimensions and improve the material quality. Hence, the MCD method is the globally preferred method for SCF production, especially for the nonlinear parametric applications, which form the focus of this paper.

The main steps of the MCD process are depicted in Fig. 1(a). Firstly, a silicon rod is sleeved into a silica tube, of which one end has been sealed to form a preform. In order to avoid oxide dissolution from the silica cladding into the silicon core, a thin layer of calcium oxide (CaO) is used as a diffusion barrier. This barrier is also useful as it helps to reduce cracking and separation between the core and the cladding due to thermal expansion mismatch [24]. Thus the use of a CaO interface layer ultimately helps to achieve smaller drawn SCF core sizes. Secondly, the whole preform is loaded into a furnace at the top of the draw tower. The temperature of the furnace is set above both the glass transition temperature of the cladding and the melting point of the silicon core. Finally, the preform is drawn down to produce SCFs with outer diameters on the order of  $\sim 150 \mu\text{m}$  and core diameters typically around  $10 \mu\text{m}$ , as shown by the microscope image of an as-drawn SCF facet in Fig. 1(c). During the drawing process, the silicon rod is molten, but the softened cladding acts as a viscous crucible to retain the cylindrical geometry. The molten silicon solidifies into a polycrystalline form as the fiber is drawn and cools, with grain sizes of a few hundreds of micrometers to millimeter dimensions. The resulting as-drawn SCFs typically have linear losses between 4 - 10 dB/cm at telecom wavelengths [24].

To reduce the micrometer sized as-drawn SCF cores down to the smaller dimensions desired for nonlinear applications, a tapering procedure is applied, post-draw, as shown in Fig. 1(b). The as-drawn SCF is heated by the filament to reach a temperature at which the silicon core melts and the silica cladding softens. By pulling the fiber ends in opposite directions, the as-drawn SCF is stretched down to the desired dimension. The process is very similar to the fiber drawing method, however, in this case it is possible to have much greater control over the drawing speed, to more accurately tailor the fiber dimensions and the heating/cooling dynamics to improve the crystalline quality of the core. The result is tapered SCFs with dimensions that vary precisely along the length and optical losses down to  $\sim 2$  dB/cm [14], [15]. A longitudinal microscope image of a tapered SCF is shown in Fig. 1(d), in which a SCF with  $10 \mu\text{m}$  core size was tapered down to achieve a core of around  $1 \mu\text{m}$ . Fig. 1(e) shows a cross-sectional microscope image of a tapered submicron core SCF.

Although this basic tapering approach works well for obtaining core sizes in the region of  $1 - 2 \mu\text{m}$ , which are preferred for applications in the mid-infrared regime [19], in order to reach the submicron-sized cores required for nonlinear

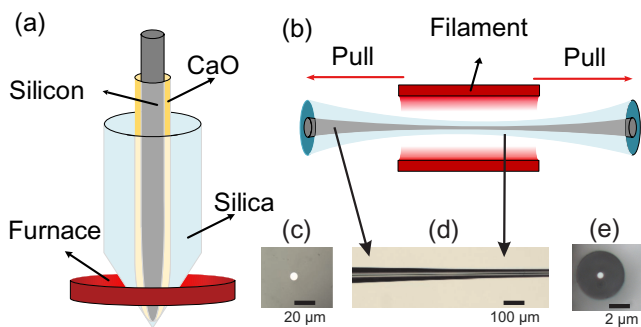
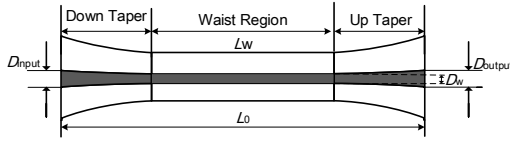


Fig. 1. (a) Schematic of the MCD method with a CaO interface modifier. (b) Schematic of the SCF tapering procedure. Microscope cross-sectional images of (c) an as-drawn SCF and (e) a tapered SCF. (d) A longitudinal image of a tapered SCF.

processing at telecoms wavelengths, a two-step tapering process has been developed [18]. In this process, the as-drawn SCFs are first tapered to obtain cladding/core diameters of  $\sim 70\ \mu\text{m}/7\ \mu\text{m}$  over a constant length of a few centimeters. A second tapering step is then applied to reach the submicron core sizes. Compared with single step tapering, the filament temperature used in this two-step process is much lower, which allows for the production of a continuous silicon core with large crystalline grains and reduced residual stress [25]. Three tapered SCFs are used in this paper and their parameters are summarized in Table I.

TABLE I  
PARAMETERS FOR THREE SUBMICRON TAPERED SCFS.



Label	Fiber 1	Fiber 2	Fiber 3
Waist diameter $D_w$ (nm)	850	850	915
Waist length $L_w$ (mm)	5	10	5
Total length $L_0$ (mm)	9	14	8
Input diameter $D_{\text{input}}$ ( $\mu\text{m}$ )	5	5	4.6
Output diameter $D_{\text{output}}$ ( $\mu\text{m}$ )	4.6	4.6	4.0
Transmission $\alpha$ (dB)	8.6	9.5	9.5
Linear loss $\alpha_l$ (dB/cm)	2.0	1.9	2.8

As shown by the schematic design of the tapered SCFs at the top of Table I, all of these fibers include a uniform straight waist region, of a particular length, and two transition regions, the down-taper transition and up-taper transition, respectively. By maintaining relatively slowly varying transition regions, coupling between the various modes supported by the submicron-sized cores and/or the radiation modes of the cladding will be minimal. Larger core sizes at the taper input and output help to improve the coupling efficiencies. As seen in the schematic of Table I,  $D_w$  is the silicon core diameter of the waist region,  $L_w$  is the length of the waist,  $L_0$  is the total length of the SCF, and  $D_{\text{input/output}}$  is the core diameter at the input/output facet of the tapered SCF.

The values for the total transmission loss ( $\alpha$ ) of the SCFs were measured using a CW laser at a wavelength of 1550 nm. The linear losses ( $\alpha_l$ ) of the tapered waist are then estimated by subtracting the coupling losses ( $\sim 7$  dB) from the total transmission and dividing by the length of the SCF. As it can be seen from Table I, all of the three tapered submicron SCFs exhibited linear losses lower than 3 dB/cm, which is a typical benchmark required for efficient nonlinear transmission. The propagation loss of Fiber 2 is estimated to be  $\sim 1.9$  dB/cm, which, so far, represents the lowest value reported for any polysilicon fiber, or indeed polysilicon planar waveguide, with submicron dimensions in the telecoms band [14], [21]. Moreover, as the crystallinity of the silicon core material has

been shown to improve with decreasing diameter [15], this loss value represents an upper bound on the loss in the tapered waist, which is considerably smaller than the input and output transitions, and where nonlinear processing occurs. One can expect that continued optimization of the material quality and tapering processes could further improve the crystallinity of the silicon core, and eventually reduce the losses of the SCFs to  $< 1$  dB/cm.

### III. THEORY OF FOUR-WAVE MIXING

FWM arises due to the third order nonlinearity  $\chi^{(3)}$  of a material, which, in this case, is the silicon fiber core. In this paper only degenerate FWM is considered, where two identical photons from a pump wave (at frequency  $\omega_p$ ) are converted to a signal photon  $\omega_s$  and an idler photon  $\omega_i$ . The generated signal photons will amplify the incident signal beam, while the idler photons generate a beam at a new frequency. Efficient FWM processes occur when both energy conservation and momentum conservation are satisfied. The conservation of energy is expressed as follows:

$$2\omega_p = \omega_s + \omega_i, \quad (1)$$

it determines the frequency of the idler and is straightforward to achieve. Conservation of momentum, however, is more difficult to satisfy and requires minimal phase mismatch between the pump, signal, and idler waves. The phase mismatch term  $\Delta k$  can be expressed as:

$$\Delta k = \Delta k_L + \Delta k_{NL}, \quad (2)$$

where  $\Delta k_L$  and  $\Delta k_{NL}$  are the linear and nonlinear phase mismatch, respectively.  $\Delta k_{NL}$  arises due to changes in the refractive index induced by the high power pump wave and is defined as:

$$\Delta k_{NL} = 2\gamma P_p, \quad (3)$$

where  $\gamma = 2\pi n_2/\lambda_p A_{\text{eff}}$  is the effective nonlinearity parameter ( $n_2$  is the nonlinear refractive index,  $\lambda_p$  is the pump wavelength, and  $A_{\text{eff}}$  is the effective mode area) and  $P_p$  is the pump peak power. The linear phase mismatch  $\Delta k_L$  is related to the fiber dispersion, which can be expanded in a power series around the pump frequency [26]. For pump wavelengths close to the zero dispersion wavelength (ZDW), both the group velocity dispersion (GVD,  $\beta_2$ ) and the fourth order dispersion (FOD,  $\beta_4$ ) terms need to be considered [27],

$$\Delta k_L = \beta_2 \Delta\omega^2 + \beta_4 \Delta\omega^4/12, \quad (4)$$

where  $\Delta\omega = |\omega_p - \omega_s|$  is the frequency difference between the signal and the pump waves. As mentioned, efficient FWM occurs when the phase mismatch term  $\Delta k$  equals, or is close to zero. Because the nonlinear term  $\Delta k_{NL}$  is positive, it requires a negative linear term  $\Delta k_L$ , determined by the magnitudes and signs of  $\beta_2$  and  $\beta_4$ .

Fig. 2(a) presents the simulated mode profiles of the fundamental mode in two SCFs with core diameters of 850 and 915 nm, at a pump wavelength of 1.55  $\mu\text{m}$ , obtained via finite element method (FEM) modelling. It can be seen that both of these fundamental modes are well confined in the silicon core. The GVD and FOD dispersion of the SCFs are calculated

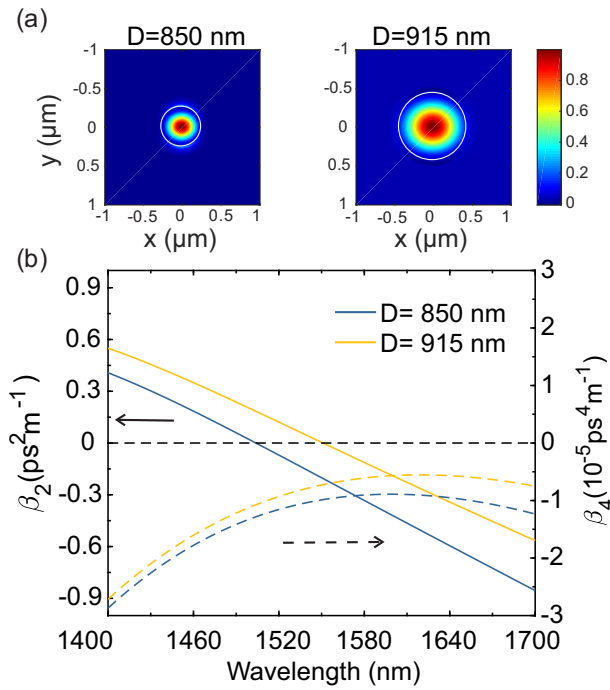


Fig. 2. (a) Simulated mode profiles of different core diameter ( $D_w=850$  nm and  $915$  nm) fibers at a wavelength of  $1.55 \mu\text{m}$ . White lines highlight the boundary between the silicon core and silica cladding. (b) Calculated GVD (solid lines) and FOD (dashed lines) dispersion as a function of wavelength for the SCFs with the different core diameters, as labelled in the legend.

using the refractive indices of silicon and silica from the literature [28], [29], and shown in Fig. 2(b). The ZDW of the SCF shifts to shorter wavelengths as the core size is reduced. When  $\Delta k_L = 0$ , then

$$\Delta\omega = \sqrt{\frac{12|\beta_2|}{|\beta_4|}}. \quad (5)$$

This means that a larger conversion bandwidth can be obtained when higher order dispersion  $\beta_4$  is included. As the values of  $\beta_4$  in these SCFs are negative across the entire telecom band, both positive and negative  $\beta_2$  could satisfy the phase matching condition, and allow for broadband gain [30].

With the assumption of an undepleted pump and a strong signal beam, the conversion efficiency (CE) of the idler wave

TABLE II  
NONLINEAR PARAMETERS OF THE TAPERED SCFS

Core diameter (nm)	850	915
$A_{\text{eff}} (\mu\text{m}^2)$	0.31	0.36
$\gamma (\text{W}^{-1}\text{m}^{-1})$	52.1	45.47
$\beta_2 (\text{ps}^2/\text{m})$	-0.158	0.042
$\beta_4 (10^{-5} \text{ps}^4/\text{m})$	-1	-0.73

is expressed as [26],

$$CE = \frac{P_{\text{idler}}^{\text{out}}}{P_{\text{signal}}^{\text{in}}} = \left[ \frac{\gamma P_p}{g} \sinh(gL_{\text{eff}}) \right]^2, \quad (6)$$

where  $P_{\text{idler}}^{\text{out}}$  is the output power of the idler wave,  $P_{\text{signal}}^{\text{in}}$  is the input power of signal wave,  $L_{\text{eff}} = (1 - e^{-\alpha_l L})/\alpha_l$  is the effective fiber length, taking into account the linear propagation loss, and the parametric gain coefficient  $g$  is given by [31]:

$$g = \sqrt{\gamma P_p \Delta k_L - (\Delta k_L/2)^2}. \quad (7)$$

Fig. 3(a) and (b) show the simulated conversion efficiency as a function of the SCF length and signal wavelength, when pumped at  $1.54 \mu\text{m}$  for the  $850$  nm and  $915$  nm fiber core size, respectively. The parameters used in the simulations are listed in Table II [16]. As shown in Fig. 3(a) and (b), high-order phase matched bands can be observed in both SCFs. The conversion bandwidth increases from  $172$  nm to  $708$  nm, as the core diameter of SCF changes from  $850$  nm to  $915$  nm, when the tapered waist length corresponds to that of Fibers 1 and 3 ( $L_w = 5$  mm). Moreover, the maximum conversion efficiency can reach  $\sim 30$  dB when the SCF length is  $10$  mm, as in Fiber 2. However, the bandwidth ( $123$  nm) is slightly narrower than that achieved in Fiber 1, which has a shorter length. In general, a larger conversion bandwidth can be achieved with a decrease in fiber length, but at the cost of a lower conversion efficiency. Fig. 3(c) shows the contour map of conversion efficiency as a function of pump and signal wavelengths, with a SCF waist length of  $10$  mm. When the high-order phase matched bands merge with the fundamental band, a maximum conversion

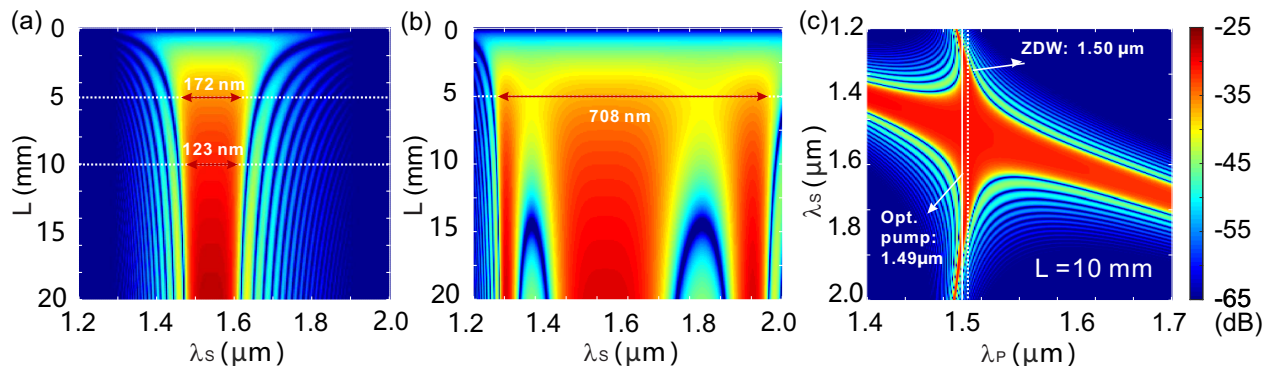


Fig. 3. Simulated conversion efficiency as a function of SCF length and signal wavelength, pumping at  $1.54 \mu\text{m}$ . (a) Fiber 1 and 2 ( $D_w = 850$  nm) and (b) Fiber 3 ( $D_w = 915$  nm). (c) Calculated conversion efficiency as a function of pump and signal wavelengths in Fiber 2 ( $D_w = 850$  nm), with a length of  $10$  mm.



bandwidth can be obtained. This can be realized by fine tuning the pump wavelength in the vicinity of the ZDW. The optimum pump wavelength for Fiber 2 is around 1495.2 nm. As shown in Fig. 2, the submicron SCFs exhibit negative  $\beta_4$  values over a pump wavelength range from 1400 nm to 1700 nm, and a conversion bandwidth of over 60 nm is achievable across the entire tuning bandwidth.

#### IV. EXPERIMENTAL DEMONSTRATIONS

Depending on the pumping scheme, both wavelength conversion and parametric amplification can be demonstrated based on the FWM processes. As discussed in Section III, the phase matching conditions can be satisfied in the submicron core SCFs over the extended telecoms bands. Hence, wavelength conversion and optical parametric amplification are investigated using the three tapered SCFs listed in Table I to establish their potential for application in nonlinear signal processing.

##### A. Experimental Setup

Fig. 4 shows the setup for the basic FWM experiments. The pump and signal beams are combined using a 3 dB optical coupler (OC), and then free space coupled into the tapered SCFs. Two polarization controllers (PC) are used to adjust the polarization of the two waves for optimising the conversion efficiency. In order to match the mode size at the input facet of the tapered SCFs, a 40 $\times$  objective lens (OL) with  $NA = 0.65$  was chosen to optimize coupling into the fundamental mode of the SCF [32]. No additional polarizer was needed in the input coupling as the cylindrically symmetric SCFs are polarization insensitive. The output light is collected by a tapered lens fiber (TLF,  $NA = 0.40$ ), or a second microscope objective lens (OL2) with  $NA = 0.85$ . The output power was measured using a power meter (Thorlab S148C) and the spectrum recorded with an optical spectrum analyzer (OSA Yokogawa AQ6370D), operating at a 1 nm resolution bandwidth.

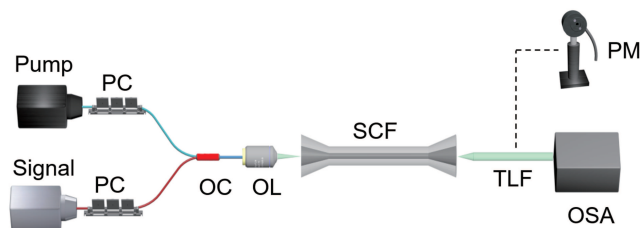


Fig. 4. The experimental setup for FWM in the tapered SCFs. PC, polarization controller; OC, optical coupler; OL, objective lens; TLF, tapered lens fiber; OSA, optical spectrum analyzer; PM, power meter.

##### B. Wavelength Conversion

For the wavelength conversion experiments, a tunable CW laser operating in the C-band was used as the pump source. An erbium-doped fiber amplifier (EDFA) was used to boost the average pump power and a tunable band-pass filter (BPF) inserted to suppress the amplified spontaneous emission (ASE) noise caused by the EDFA. To investigate the bandwidth of the

wavelength conversion, a second tunable CW laser covering 1500 – 1680 nm was used as a signal wave. The conversion efficiency can be extracted from the output spectra using the definition given by Eq. (6). Fiber 1 and Fiber 2, which have the same waist diameter (850 nm) but different lengths, were investigated in the wavelength conversion experiments. For comparison, the coupled input pump power was kept the same at 18 dBm. The maximum conversion efficiency obtained in Fiber 2 ( $\sim -30$  dB) was larger than that of Fiber 1 ( $\sim -35$  dB), which can be attributed to its longer length. The maximum conversion efficiency stays at a similar value when the pump wavelength changes from 1540 nm to 1560 nm.

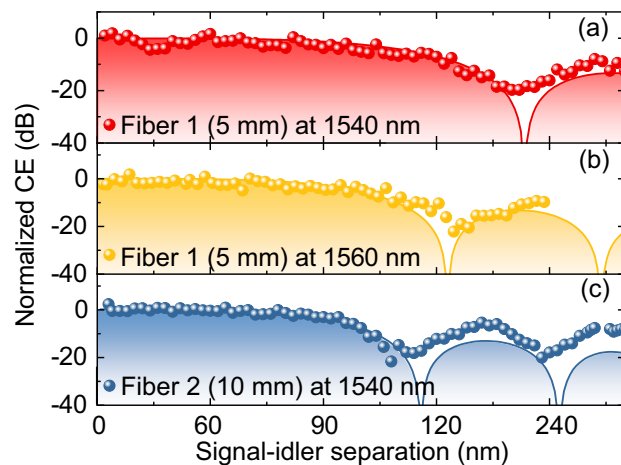


Fig. 5. Measured FWM conversion efficiency (normalized) as a function of signal-idler wavelength separation for different tapered SCFs at selected pump wavelengths, given in the legend. (a) Fiber 1 ( $L_w = 5$  mm) pumped at 1540 nm, (b) Fiber 1 pumped at 1560 nm, and (c) Fiber 2 ( $L_w = 10$  mm) pumped at 1540 nm. Solid lines and shaded area show the simulation results.

Fig. 5 shows the normalized conversion efficiency as a function of signal-idler wavelength separation, and at different pump wavelengths, for the two tapered SCFs. Wavelength conversion can be observed when the signal-idler wavelength separation is over 260 nm (corresponding to when the CW signal is tuned to 1680 nm), which is consistent with the simulations shown in Fig. 3(a). These results suggest that broadband wavelength conversion (more than 260 nm) can be achieved in the tapered SCFs, covering the entire S-, C-, and L- telecom bands. It is important to note that this experimental conversion bandwidth was only limited by the tuning range of the CW signal source. In order to compare the conversion bandwidth, a 3 dB bandwidth is defined using the separation of the signal and idler wavelengths and noting when the conversion efficiency drops to half of its maximum value. As it can be seen from Fig. 5, Fiber 1 exhibits the largest 3 dB bandwidth (144 nm) when pumped at 1540 nm. As the pump wavelength moves further from the ZDW (1502 nm) to 1560 nm, the bandwidth reduces slightly to 122 nm. This suggests that Fiber 1 maintains a broad bandwidth when the pump wavelength is tuned across the telecom C-band, owing to its relatively flat GVD slope close to the ZDW. Although Fiber 2 supports a higher conversion efficiency, its conversion bandwidth ( $\sim 120$  nm) is narrower, due to walk-off between the signal and pump waves caused by the longer fiber length.

Nevertheless, this conversion bandwidth is still slightly larger than most previous reports in silicon nanowire waveguides using a telecom pump source [31], with the only exception being a specially designed rib waveguide structure [33].

In order to verify the relationship between the conversion efficiency and the dispersion properties of the tapered SCFs, the theoretical conversion efficiency was calculated using the estimated dispersion values of  $\beta_2 = -0.17 \text{ ps}^2/\text{m}$ ,  $\beta_4 = -1.03 \times 10^{-5} \text{ ps}^4/\text{m}$  at 1540 nm and  $\beta_2 = -0.25 \text{ ps}^2/\text{m}$ ,  $\beta_4 = -0.95 \times 10^{-5} \text{ ps}^4/\text{m}$  at 1560 nm, which are the same for both fibers. As shown by the shaded areas in Fig. 5, the simulated curves are in reasonable agreement with the measured conversion efficiencies. We attribute the slight mismatch of the sidebands to discrepancies in the estimated FOD values of the SCFs and the detection sensitivity of the OSA.

### C. Optical Parametric Amplification

If a high power pump is combined with the signal beam during the FWM process, the signal can experience significant parametric amplification. OPA has been studied extensively in both silica-based HNLFs and planar silicon waveguides. Previous work using planar silicon waveguides has shown that parametric gain in silicon waveguides saturates at high input powers due to two-photon absorption (TPA)-induced free carrier absorption (FCA) in the telecom band [4]. Thus, using short pulsed pump sources is favoured when using silicon for OPA demonstrations in order to reduce the free carrier absorption. In the experiments discussed here, a mode locked erbium doped fiber laser with a pulse duration of  $T_{\text{fwhm}} = 670 \text{ fs}$  was employed as the pump source, operating at  $\lambda_p = 1541 \text{ nm}$  and a 40 MHz repetition rate. For this fixed pump wavelength, Fiber 3, with a core diameter of 915 nm and a waist length of 5 mm was chosen, as it has a very small positive GVD ( $\beta_2 \sim 0.04 \text{ ps}^2 \text{ m}^{-1}$ ) and a negative FOD ( $\beta_4 \sim -0.8 \times 10^{-5} \text{ ps}^4 \text{ m}^{-1}$ ). From Eq. (5), the dispersion

profile of Fiber 3 could permit broadband phase matching over a conversion bandwidth of  $\sim 708 \text{ nm}$ .

As can be seen from the inset of Fig. 6(a), a moderate coupled average pump power of  $\sim 0.63 \text{ mW}$  ( $\sim 17 \text{ W}$  peak power) was chosen, as this was just below the TPA saturation threshold and also before the spectrum undergoes broadening due to SPM. OPA was studied for a range of CW signals covering 1500 – 1680 nm, and the measured overlaid FWM spectra including the amplified signals, generated idlers and the pumps are plotted in Fig. 6(a). It is worth noting that both the amplified signals and generated idlers occur as a train of pulses with similar durations and repetition rates to that of the pump pulses. Hence, the parametric signal gain and the idler conversion gain can be extracted by converting the time-averaged power to the peak power weighted by the duty cycle factor  $F = 1/(40 \text{ MHz} \cdot 670 \text{ fs})$ , following the same method used in Refs. [4], [34]. The extracted values of the idler conversion gain and parametric signal gain are plotted in Fig. 6(b) and Fig. 6(c), respectively. For both the signal and idler beams, the gains decrease as the signal wavelength moves away from the pump, which follows the theoretical predictions for waveguides pumped in the normal dispersion region [35]. The maximum signal gain of  $\sim 9.3 \text{ dB}$  is achieved for a signal wavelength at 1570 nm, with a corresponding idler conversion gain of  $\sim 8.5 \text{ dB}$ . To the best of our knowledge, this is currently the highest gain recorded in a crystalline silicon waveguide using a telecom pump; facilitated by the low transmission losses of the tapered SCF and the use of femtosecond pump pulses to reduce free carrier effects [4]. Moreover, it is worth noting that a 2 dB net off-waveguide gain has been obtained for the first time in any silicon waveguide, thanks to the relatively low insertion losses (7 dB) of the tapered SCFs compared to the planar nanowires. Even higher gains could be obtained by further reduction in the transmission losses and increased lengths of the tapered SCFs. Similar to the carrier sweep-out scheme developed in planar silicon waveguides, we anticipate that amplification of practical optical data signals

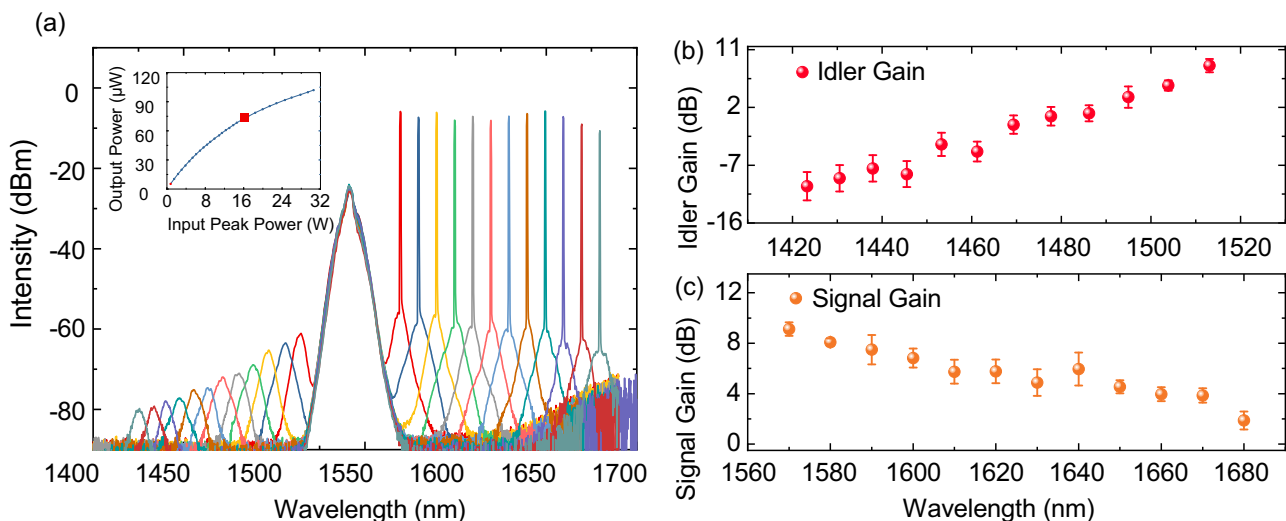


Fig. 6. (a) Transmission spectra taken at the output of the SCF as the signal wavelength is tuned from 1570 to 1680 nm. The inset shows the output power as a function of the input coupled pump peak power. (b) Idler gain and (c) signal gain as a function of wavelength. The error bars in the parametric gain data are derived from the uncertainty in the total propagation loss and the OSA noise. This figure is replotted from [18].

will be possible by building a PIN structure into the SCF [36], [37]. Alternatively, as suggested by Fig. 3(b), the OPA gain bandwidth could even be extended into the  $2\ \mu\text{m}$  wavelength region by utilizing the FOD related phase matching condition, which would help to mitigate issues with nonlinear losses, and work in this area is ongoing.

## V. SIGNAL PROCESSING AND FUTURE PROSPECTS

FWM-based wavelength conversion is the most widely investigated nonlinear effect for all-optical signal processing in optical communications. As FWM takes place at ultrafast time-scales, it is possible to convert high-speed amplitude and phase modulated optical signals directly to the corresponding idler wavelengths. In this section, all-optical signal processing of 20 Gb/s data signals using a tapered SCF will be described, and potential solutions for all-fiber integrated nonlinear devices discussed.

### A. Signal Processing of 20 Gb/s Data Signal

Fig. 7 shows the experimental setup for FWM-based wavelength conversion of widely used QPSK signals. Fiber 3 is used in the experiments as it exhibited almost constant conversion efficiency for both C and L signal wavelengths, which can be seen from Fig. 3(b). The CW pump originates from a laser emitting light at 1550 nm, which is then amplified by a high-power EDFA, with a BPF inserted to suppress the ASE noise. QPSK optical signals are generated at 10 Gbaud using an arbitrary waveform generator (AWG) at both 1563 nm (C-band) and 1580 nm (L-band). The modulated QPSK signals are then amplified by a second EDFA. Two polarization controllers (PCs) are used to align the polarization states of the pump and signal waves to achieve the maximum conversion efficiency. The pump and modulated signal are then combined together by a 50:50 OC and free space coupled into the SCF using a  $40\times$  objective lens (OL1). The output is coupled out from the SCF by another objective lens (OL2,  $63\times$ ) and sent for detection. A 99:1 tap coupler is used to accurately monitor the output power and spectrum via an OSA. The converted idlers

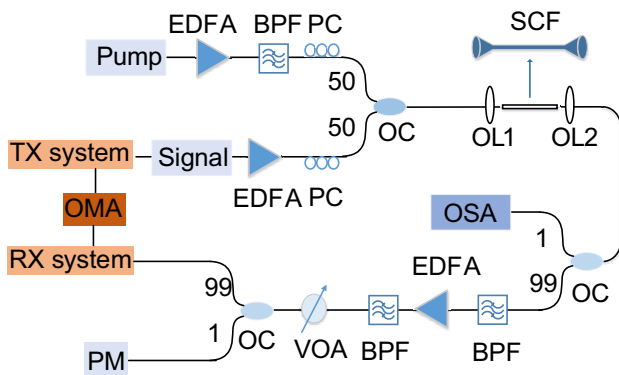


Fig. 7. The experimental setup for signal processing of 20 Gb/s QPSK signals. OMA, optical modulation analyzer; BPF, band pass filter; PC, polarization controller; OC, optical coupler; OL, objective lens; OSA, optical spectrum analyzer; VOA, variable optical attenuator; PM, power meter.

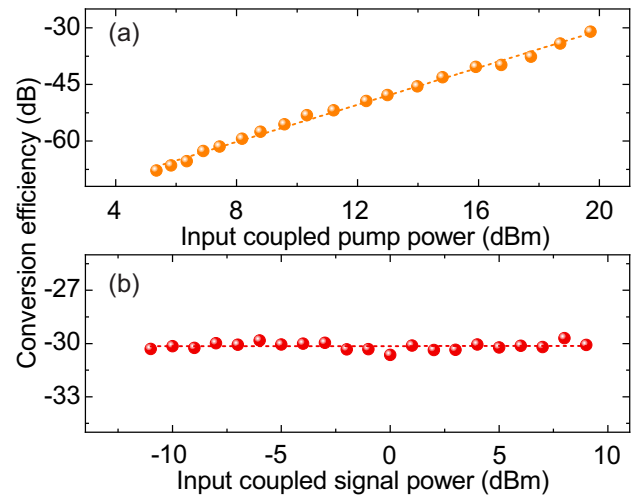


Fig. 8. (a) Conversion efficiency as a function of coupled input pump power with an input signal power of 9 dBm. (b) Conversion efficiency as a function of coupled input signal power with an input coupled pump power of 20 dBm. The pump and signal wavelengths are 1550 nm and 1563 nm, respectively.

are selected using the second BPF and sent to a third EDFA, followed by a third BPF, which is used to suppress the ASE noise from the EDFA. The received power level is controlled using a variable optical attenuator (VOA). Finally, the output is measured by a power meter and sent to an optical modulation analyzer (OMA) that allowed assessment of the wavelength conversion, both in terms of constellation diagrams and bit error ratio (BER) measurements.

To investigate the optimum pump power for FWM wavelength conversion, the efficiency in Fiber 3 is plotted as a function of coupled pump power with the signal wavelength set at 1563 nm in Fig. 8(a). It can be seen that the conversion efficiency increases linearly from  $-67.8\ \text{dB}$  to  $-30.1\ \text{dB}$  as the coupled pump power is raised from 5.4 dBm to 19.5 dBm. Fig. 8(b) shows that the conversion efficiency remains constant when the signal power is varied from  $-11\ \text{dBm}$  to 9 dBm for a pump power of 19.5 dBm, which suggests that the nonlinear

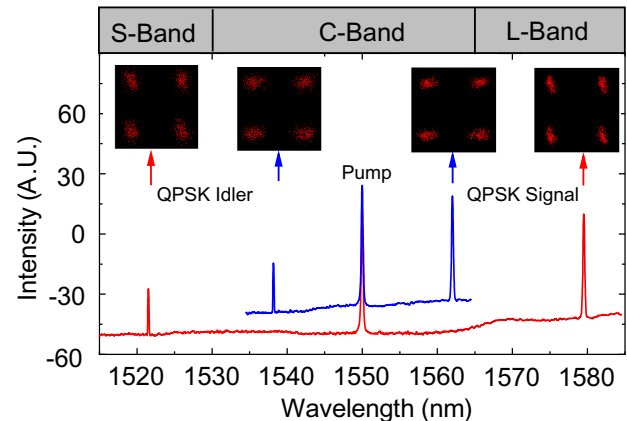


Fig. 9. Measured spectra for wavelength conversion of 20 Gb/s QPSK data at two signal wavelengths; 1563 nm and 1580 nm. The FWM spectra are offset by 10 dB. Insets show the constellation diagrams for the original and converted signals.

losses are negligible at this power level. Hence, the coupled optical powers of the signals and the pump in the experiments that follow were set to be 9 dBm and 19.5 dBm, respectively.

Fig. 9 shows the optical spectra measured at the output of the tapered SCF, for the two modulated signals in the C- and L-bands. Both back to back (B-to-B) and converted idler constellation diagrams are recorded by the OMA and plotted in the insets of Fig. 9, clearly indicating that the modulated data has been successfully converted with additional noise. The quality of this SCF-based signal processing system was evaluated by measuring the BER of the converted idler and the original signal, at the receiver as a function of the received optical power, with the results shown in Fig. 10. Although the signal output power is relatively low, which is due both to the low collection efficiency and the insertion losses of the cascaded BPF, the BER results reveal that a successful conversion has been achieved with a power penalty of 1 to 2 dB at a BER of  $3.8 \times 10^{-3}$  (the hard-decision forward error correction (HD-FEC) limit) for signals in both the L- and C-bands. We anticipate that successful high-speed wavelength conversion of more advanced signals could be demonstrated in our SCFs with improved conversion efficiency and coupling. Moreover, the conversion of broad, THz bandwidth, data signals should also be achievable via careful optimization of the inter-channel crosstalk in our future work. Thus these results highlight the potential for SCFs to find use in practical telecom applications.

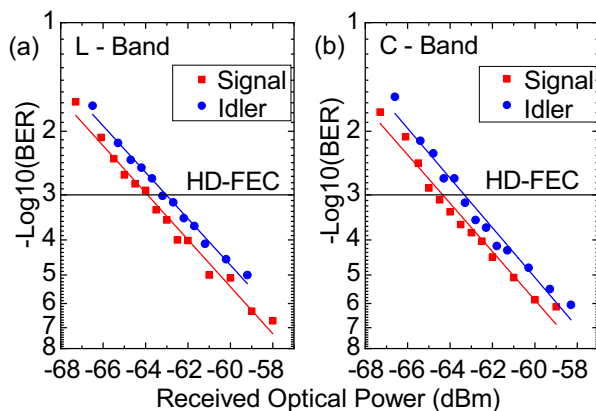


Fig. 10. BER curves as a function of the received optical power for the 20 Gb/s QPSK data for signals in the (a) L-band and (b) C-band.

### B. Towards All-fiber Integrated Nonlinear Devices

Because of the high refractive index of silicon, efficient light coupling into silicon waveguides has long been regarded as a difficult task, which hinders the practical application of any silicon-based nonlinear device. Despite the fact that SCFs have physical similarity to single mode fibers (SMFs), to date, most of the nonlinear demonstrations have employed free space systems to couple the pump light into the SCFs, due to issues associated with the high index core. However, recently a more efficient method of optical coupling has been established by tapering a nano-spike structure on to the end of the SCFs [38], similar to the well-established inverse taper approach

used for planar nanowire waveguides [39]. Importantly, this has opened a route to directly splice the SCFs to standard silica-based fibers to produce a robust and efficient all-fiber system, as illustrated in Fig. 11(a). In this approach, both the SCF and SMF are tapered to improve the mode coupling, as well as to better match the fiber dimensions as shown in the schematic.

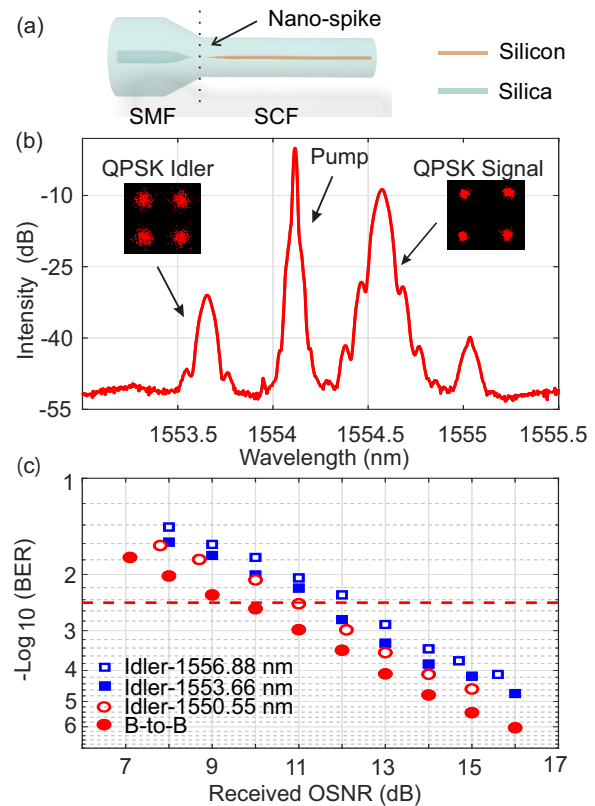


Fig. 11. (a) Schematic of a SMF-SCF all-fiber device with a nano-spike coupler. (b) QPSK spectrum recorded at the output of the wavelength converter. Inset: signal and idler constellation diagrams. (c) BER measurements of 20 Gb/s QPSK data at different idler wavelengths and B-to-B signal wavelengths. This figure is replotted from [40].

In order to evaluate the potential of such an all-fiber integrated device, a SCF with tapered nano-spike was fabricated and spliced to a SMF input coupler and investigated for use as a nonlinear wavelength converter (NWC). Although submicron core sized SCFs are favored for wavelength conversion, as discussed in Section III, there are significant challenges to fabricating integrated devices with such small cores owing to the associated micrometer-sized outer diameters ( $< 20 \mu\text{m}$ ), which are too small to be held in the splicing rig. Thus, as a proof-of-concept, the fabricated device made use of a tapered SCF with a  $\sim 1.1 \mu\text{m}$  core diameter and a  $30 \mu\text{m}$  cladding diameter. The final fabricated SCF-NWC consisted of a 1.1 cm long SCF with a  $200 \mu\text{m}$  long nano-spike, connected to a SMF pigtail with a 4 mm long tapered transition region to facilitate mode coupling between the two structures. Fabrication details can be found in Ref. [38]. During the fabrication, all the heat-polishing, tapering, and splicing steps are undertaken using a commercial silica fiber processing workstation (Vytran GPX-3400-V4), owing to the compatibility of the SCF platform with



conventional silica fiber post-processing procedures. The total insertion loss of the SCF with a nanospike coupler is around 11 dB. Cut-back measurements reveal the linear transmission loss of the SCF to be  $\sim 2$  dB/cm, from which we can estimate the nano-spike coupling loss to be around 4.5 dB [40].

The experimental setup for wavelength conversion in this device is similar to that depicted in Fig. 7, except that the input of the fabricated SCF-NWC is directly connected to the fiber-based pump and signal sources. A 20 Gb/s QPSK signal was modulated on the signal wave before coupling into the SCF-NWC, and the output spectra and constellations are shown in Fig. 11(b). These results show that the modulated data has been successfully converted to the idler wavelength. The BER performances are also evaluated as a function of optical signal to noise ratio (OSNR), plotted in Fig. 11(c), clearly indicating that the conversion is achieved with negligible OSNR penalties (1 to 2 dB) for selected wavelengths in the C-band. We note that although the FWM bandwidth of this SCF-NWC is narrower in the telecoms band than those of the submicron SCFs used in the previous section, owing to its larger, normal GVD parameter in this region, it could be exploited for applications beyond  $2 \mu\text{m}$  where the  $\sim 1.1 \mu\text{m}$  core will exhibit anomalous dispersion [18]. Interestingly, the SCF-NWC devices are well suited to broadband operation as the nano-spike couplers operate over a wide wavelength range [41]. Thus, this work highlights the potential of the SCF platform to form the basis of robust all-fiber integrated nonlinear components, which represent an interesting solution for all-optical signal processing systems, across the telecoms band and beyond.

## VI. CONCLUSION

This paper has reported on the recent progress in nonlinear wavelength conversion and OPA using tapered SCFs. Fibers with submicron-sized cores have been fabricated from SCFs produced via the MCD method by applying a post-draw tapering procedure. Using SCFs with carefully designed dispersion profiles, FWM-based wavelength conversion has been demonstrated with bandwidths covering the entire telecom band and parametric amplification has been achieved with a gain as high as 9 dB using only a moderate pump peak power. Moreover, all-optical signal processing of 20 Gbit/s data signals has been demonstrated over the extended telecom region (S-, C-, and L-bands). Clearly, low loss, all-fiber integration as demonstrated through the SCF-NWC device would greatly improve the efficiency and practicality of the FWM solutions.

It is worth noting that the SCF all-optical signal processing demonstrations presented in this review are still in their early stages of development. Moreover, they represent only a subset of this rapidly growing field, and currently there are several high performance solutions emerging that make use of integrated waveguide structures with novel waveguide designs [42], new nonlinear materials [43], [44], and involve innovative fabrication techniques [45], [46]. However, with continued advancements to reduce the material losses and improve the device efficiency, we anticipate that these SCFs will provide a versatile platform for nonlinear signal processing applications within next-generation telecommunication systems.

## ACKNOWLEDGMENT

The authors would like to thank their colleagues and collaborators who contributed to the cited work. The authors acknowledge Mr Meng Ding and Prof. Radan Slavik for fruitful discussions and the use of their equipment.

## REFERENCES

- [1] J. Hansryd, P. A. Andrekson, M. Westlund, and P. Hedekvist, "Fiber-based optical parametric amplifiers and their applications," *IEEE J. Sel. Top. Quantum Electron.*, vol. 8, no. 3, pp. 506–520, 2002.
- [2] H. Kishikawa, N. Goto, and L. R. Chen, "All-optical wavelength-preserved modulation format conversion from PDM-QPSK to PDM-BPSK using FWM and interference," *J. Lightwave Technol.*, vol. 34, no. 23, pp. 5505–5515, 2016.
- [3] K. K. Chow, C. Shu, C. Lin, and A. Bjarklev, "Polarization-insensitive widely tunable wavelength converter based on four-wave mixing in a dispersion-flattened nonlinear photonic crystal fiber," *IEEE Photon. Technol. Lett.*, vol. 17, no. 3, pp. 624–626, 2016.
- [4] M. A. Foster, A. C. Turner, J. E. Sharping, B. S. Schmidt, M. Lipson, and A. L. Gaeta, "Broad-band optical parametric gain on a silicon photonic chip," *Nature*, vol. 441, pp. 960–963, 2006.
- [5] M. A. Ettabib, K. Hammani, F. Parmigiani, L. Jones, A. Kapsalis, A. Bogris, D. Syvridis, M. Brun, P. Labeye, S. Nicoletti, and P. Petropoulos, "FWM-based wavelength conversion of 40 Gbaud PSK signals in a silicon germanium waveguide," *Opt. Express*, vol. 21, no. 14, pp. 16683–16689, 2013.
- [6] B. Kuyken, S. Clemmen, S. K. Selvaraja, W. Bogaerts, D. V. Thourhout, P. Emplit, S. Massar, G. Roelkens, and R. Baets, "On-chip parametric amplification with 26.5 dB gain at telecommunication wavelengths using CMOS-compatible hydrogenated amorphous silicon waveguides," *Opt. Lett.*, vol. 36, no. 4, pp. 552–554, 2011.
- [7] B. J. Eggleton, B. Luther-Davies, and K. Richardson, "Chalcogenide photonics," *Nature Photon.*, vol. 5, pp. 141–148, 2011.
- [8] F. Da Ros, E. Porto da Silva, D. Zibar, S. T. Chu, B. E. Little, R. Morandotti, M. Galili, D. J. Moss, and L. K. Oxenløwe, "Wavelength conversion of QAM signals in a low loss CMOS compatible spiral waveguide," *APL Photonics*, vol. 2, no. 4, pp. 046105, 2017.
- [9] K. J. A. Ooi, D. K. T. Ng, T. Wang, A. K. L. Chee, S. K. Ng, Q. Wang, L. K. Ang, A. M. Agarwal, L. C. Kimerling, and D. T. H. Tan, "Pushing the limits of CMOS optical parametric amplifiers with USRN: Si<sub>7</sub>N<sub>3</sub> above the two-photon absorption edge," *Nature Commun.*, vol. 8, no. 13878, 2017.
- [10] M. Pu, H. Hu, L. Ottaviano, E. Semenova, D. Vukovic, L. K. Oxenløwe, and K. Yvind, "Ultra-efficient and broadband nonlinear AlGaAs-on-Insulator chip for low-power optical signal processing," *Laser Photon. Rev.*, vol. 12, no. 12, pp. 1800111, 2018.
- [11] R. Salem, M. A. Foster, A. C. Turner, D. F. Geraghty, M. Lipson, and A. L. Gaeta, "Signal regeneration using low-power four-wave mixing on silicon chip," *Nature Photon.*, vol. 2, pp. 35–38, 2008.
- [12] J. Leuthold, C. Koos, and W. Freude, "Nonlinear silicon photonics," *Nature Photon.*, vol. 4, pp. 535–544, 2010.
- [13] L. K. Oxenløwe, H. Ji, M. Galili, M. Pu, H. Hu, H. C. H. Mulvad, K. Yvind, J. M. Hvam, A. T. Clausen, and P. Jeppesen, "Silicon photonics for signal processing of Tbit/s serial data signals," *IEEE J. Sel. Top. Quantum Electron.*, vol. 18, no. 2, pp. 996–1005, 2012.
- [14] F. H. Suhailin, L. Shen, N. Healy, L. Xiao, M. Jones, T. Hawkins, J. Ballato, U. J. Gibson, and A. C. Peacock, "Tapered polysilicon core fibers for nonlinear photonics," *Opt. Lett.*, vol. 41, no. 7, pp. 1360–1363, 2016.
- [15] Y. Franz, A. F. J. Runge, H. Ren, N. Healy, K. Ignatyev, M. Jones, T. Hawkins, J. Ballato, U. J. Gibson, and A. C. Peacock, "Material properties of tapered crystalline silicon core fibers," *Opt. Mater. Express*, vol. 7, no. 6, pp. 2055–2061, 2017.
- [16] A. C. Peacock, J. Campling, A. F. J. Runge, H. Ren, L. Shen, O. Aktas, P. Horak, N. Healy, U. J. Gibson, and J. Ballato, "Wavelength Conversion and Supercontinuum Generation in Silicon Optical Fibers," *IEEE J. Sel. Top. Quantum Electron.*, vol. 24, no. 3, pp. 1–9, 2018.
- [17] H. Ren, L. Shen, D. Wu, O. Aktas, T. Hawkins, J. Ballato, U. J. Gibson, and A. C. Peacock, "Nonlinear optical properties of polycrystalline silicon core fibers from telecom wavelengths into the mid-infrared spectral region," *Opt. Mater. Express*, vol. 9, no. 3, pp. 1271–1279, 2019.

- [18] D. Wu, L. Shen, H. Ren, J. Campling, T. W. Hawkins, J. Ballato, U. J. Gibson, and A. C. Peacock, "Net optical parametric gain in a submicron silicon core fiber pumped in the telecom band," *APL Photonics*, vol. 4, no. 8, pp. 086102, 2019.
- [19] H. Ren, L. Shen, A. F. J. Runge, T. Hawkins, J. Ballato, U. J. Gibson, and A. C. Peacock, "Low-loss silicon core fibre platform for mid-infrared nonlinear photonics," *Light Sci. Appl.*, vol. 8, no. 105, 2019.
- [20] J. Ballato, T. Hawkins, P. Foy, R. Stolen, B. Kokuoz, M. Ellison, C. McMillen, J. Reppert, A. M. Rao, M. Daw, S. Sharma, R. Shori, O. Stafstudd, R. R. Rice, and D. R. Powers, "Silicon optical fiber," *Opt. Express*, vol. 16, no. 23, pp. 18675–18683, 2008.
- [21] D. Kwong, J. Covey, A. Hosseini, Y. Zhang, X. Xu, and R. T. Chen, "Ultralow-loss polycrystalline silicon waveguides and high uniformity  $1 \times 12$ MMI fanout for 3D photonic integration," *Opt. Express*, vol. 20, no. 19, pp. 21722–21728, 2012.
- [22] R. M. Osgood, N. C. Panoiu, J. I. Dadap, X. Liu, X. Chen, I-Wei Hsieh, E. Dulkeith, W. M. J. Green, and Y. A. Vlasov, "Engineering nonlinearities in nanoscale optical systems: physics and applications in dispersion-engineered silicon nanophotonic wires," *Adv. Opt. Photon.*, vol. 1, no. 1, pp. 162–235, 2009.
- [23] P. J. A. Sazio, A. Amezcua-Correa, C. E. Finlayson, J. R. Hayes, T. J. Scheidemantel, N. F. Baril, B. R. Jackson, D.-J. Won, F. Zhang, E. R. Margine, V. Gopalan, V. H. Crespi, and J. V. Badding, "Microstructured optical fibers as high-pressure microfluidic reactors," *Science*, vol. 311, no. 5767, pp. 1583–1586, 2006.
- [24] E. F. Nordstrand, A. N. Dibbs, A. J. Eraker, and U. J. Gibson, "Alkaline oxide interface modifiers for silicon fiber production," *Opt. Mater. Express*, vol. 3, no. 5, pp. 651–657, 2013.
- [25] C. McMillen, G. Brambilla, S. Morris, T. Hawkins, P. Foy, N. Broderick, E. Koukharenko, R. Rice, and J. Ballato, "On crystallographic orientation in crystal core optical fibers II: Effects of tapering," *Opt. Mater.*, vol. 35, no. 2, pp. 93–96, 2012.
- [26] G. P. Agrawal, *Nonlinear Fiber Optics*, 5th ed. San Diego, CA, USA: Academic, 2013.
- [27] J. Harvey, R. Leonhardt, S. Coen, G. Wong, J. Knight, W. Wadsworth, and P. S. J. Russell, "Scalar modulation instability in the normal dispersion regime by use of a photonic crystal fiber," *Opt. Lett.*, vol. 28, no. 22, pp. 2225–2227, 2003.
- [28] H. Bach, and N. Neuroth, *The Properties of Optical Glass*, Heidelberg, Berlin, Germany: Springer, 1998.
- [29] H. H. Li, "Refractive index of silicon and germanium and its wavelength and temperature derivatives," *J. Phys. Chem. Ref. Data*, vol. 9, no. 3, pp. 561–658, 1980.
- [30] B. Kuyken, P. Verheyen, P. Tannouri, X. Liu, J. V. Campenhout, R. Baets, W. M. J. Green, and G. Roelkens, "Generation of 3.6  $\mu\text{m}$  radiation and telecom-band amplification by four-wave mixing in a silicon waveguide with normal group velocity dispersion," *Opt. Lett.*, vol. 39, no. 6, pp. 1349–1352, 2014.
- [31] M. A. Foster, A. C. Turner, R. Salem, M. Lipson, and A. L. Gaeta, "Broad-band continuous-wave parametric wavelength conversion in silicon nanowaveguides," *Opt. Express*, vol. 20, pp. 12949–12958, 2007.
- [32] A. C. Peacock, P. Mehta, P. Horak, and N. Healy, "Nonlinear pulse dynamics in multimode silicon core optical fibers," *Opt. Lett.*, vol. 37, no. 16, pp. 3351–3353, 2012.
- [33] A. C. Turner-Foster, M. A. Foster, R. Salem, A. L. Gaeta, and M. Lipson, "Frequency conversion over two-thirds of an octave in silicon nanowaveguides," *Opt. Express*, vol. 18, no. 3, pp. 1904–1908, 2010.
- [34] X. Liu, R. M. Osgood, Y. A. Vlasov, W. M. J. Green, R. M. O. Jr, Y. A. Vlasov, W. M. J. Green, R. M. Osgood, Y. A. Vlasov, and W. M. J. Green, "Mid-infrared optical parametric amplifier using silicon nanophotonic waveguides," *Nature Photon.*, no. 8, pp. 557–560, 2010.
- [35] Q. Lin, J. Zhang, P. M. Fauchet, and G. P. Agrawal, "Ultrabroadband parametric generation and wavelength conversion in silicon waveguides," *Opt. Express*, vol. 14, no. 11, pp. 4786–4799, 2006.
- [36] I. Sackey, A. Gajda, A. Peczek, E. Liebig, L. Zimmermann, K. Petermann, and C. Schubert, "1.024 Tb/s wavelength conversion in a silicon waveguide with reverse-biased p-i-n junction," *Opt. Express*, vol. 25, no. 18, pp. 21229–21240, 2017.
- [37] L. Wei, G. Hou, E. Levy, G. Lestoquoy, A. Gumennik, A. F. Abouraddy, J. D. Joannopoulos, and Y. Fink, "Optoelectronic Fibers via Selective Amplification of In-Fiber Capillary Instabilities," *Adv. Mater.*, vol. 29, no. 1, pp. 1603033, 2017.
- [38] H. Ren, O. Aktas, Y. Franz, A. F. J. Runge, T. Hawkins, J. Ballato, U. J. Gibson, and A. C. Peacock, "Tapered silicon core fibers with nano-spikes for optical coupling via spliced silica fibers," *Opt. Express*, vol. 25, no. 20, pp. 24157–24163, 2017.
- [39] V. R. Almeida, R. R. Panepucci, and M. Lipson, "Nanotaper for compact mode conversion," *Opt. Lett.*, vol. 28, no. 15, pp. 1302–1304, 2003.
- [40] M. Huang, H. Ren, O. Aktas, L. Shen, J. Wang, T. W. Hawkins, J. Ballato, U. J. Gibson, and A. C. Peacock, "Fiber integrated wavelength converter based on a silicon core fiber with a nano-spike coupler," *IEEE Photon. Technol. Lett.*, vol. 31, no. 19, pp. 1561–1564, 2019.
- [41] R. Marchetti, C. Lacava, L. Carroll, K. Gradkowski, and P. Minzioni, "Coupling strategies for silicon photonics integrated chips," *Photon. Res.*, vol. 7, no. 2, pp. 201–239, 2019.
- [42] C. Koos, P. Vorreau, T. Vallaitis, P. Dumon, W. Bogaerts, R. Baets, B. Esembeson, I. Biaggio, T. Michinobu, F. Diederich, W. Freude, and J. Leuthold, "All-optical high-speed signal processing with silicon-organic hybrid slot waveguides," *Nature Photon.*, vol. 3, pp. 216–219, 2009.
- [43] T. Gu, N. Petrone, J. F. McMillan, A. van der Zande, M. Yu, G. Q. Lo, D. L. Kwong, J. Hone, and C. W. Wong, "Regenerative oscillation and four-wave mixing in graphene optoelectronics," *Nature Photon.*, vol. 6, no. 8, pp. 554–559, 2012.
- [44] Y. Yang, J. Wu, X. Xu, Y. Liang, S. T. Chu, B. E. Little, R. Morandotti, B. Jia, and D. J. Moss, "Enhanced four-wave mixing in waveguides integrated with graphene oxide," *APL Photonics*, vol. 3, no. 12, pp. 120803, 2018.
- [45] D. J. Moss, R. Morandotti, A. L. Gaeta, and M. Lipson, "New CMOS-compatible platforms based on silicon nitride and indium tin oxide for nonlinear optics," *Nature Photon.*, vol. 7, pp. 597–607, 2013.
- [46] D. J. Wilson, K. Schneider, S. Hönl, M. Anderson, Y. Baumgartner, L. Czornomaz, T. J. Kippenberg, and P. Seidler, "Integrated gallium phosphide nonlinear photonics," *Nature Photon.*, vol. 14, pp. 57–62, 2020.

**Dong Wu** Dong Wu received the B.Eng. degree in optical information science and technology from the Wuhan University, Wuhan, China, in 2014 and the M.Phil. degrees in optical engineering from Shandong University, Jinan, China, in 2017. Since then, she has been studying for her PhD degree in the Optoelectronics Research Centre, University of Southampton, Southampton, U.K. Her main research interest is the study of the nonlinear effects in silicon core fibers.

**Li Shen** Li Shen received the B.Sc. and M.Phil. degrees from Huazhong University of Science and Technology (HUST), Wuhan, China, in 2009 and 2012, respectively, and the Ph.D. degree from the Optoelectronics Research Centre (ORC), University of Southampton, Southampton, U.K., in 2015. He is currently an associated Professor with HUST and a visiting scholar at the ORC. He has published over 30 peer review journal papers and his research interests include novel semiconductor photonic devices, silicon photonics, mid-infrared photonics.

**Haonan Ren** Haonan Ren received the B.Eng. degree in electrical engineering and electronics from the University of Edinburgh, Edinburgh, U.K., and Xiamen University, Xiamen, China, in 2015. He obtained Ph.D. in nonlinear optics at University of Southampton, U.K, in 2019. His current research interests include nonlinear fiber optics and tapered silicon core fibers.

**Meng Huang** Meng Huang received the B.Eng. degree in Electronic Science and Technology from the Harbin Institute of Technology, Harbin, China, in 2016. After that, he received the M. Eng. degree in Optical Engineering from the Huazhong University of Science and Technology, Wuhan, China, in 2019. Since 2019, he has been working toward the Ph. D. degree with the Optoelectronics Research Centre, University of Southampton, Southampton, U.K. His current research interests include nonlinear silicon photonics and semiconductor core fibers.

**Cosimo Lacava** Cosimo Lacava received the Ph.D. degree in optoelectronics and electronic engineering in 2014. He is an Assistant Professor at the University of Pavia and Visiting Research Fellow at the Optoelectronics Research Centre (ORC), Southampton, U.K. Previously, he was Senior Research Fellow at the ORC, which he left in 2019. He has authored and co-authored more than 30 peer review journal publications and he is regularly invited to disseminate his results at the most important optoelectronics conferences. His research interests are nonlinear optics, all optical signal processing, silicon photonic devices, and integrated optics.

**Joseph Campling** Joseph Campling received the B.Sc. degree in physical sciences from the Open University, Milton Keynes, U.K., in 2014, and the M.Sc. degree in frontiers of quantum technology from the University of Sussex, Brighton, U.K., in 2016. He is currently working toward the Ph.D. degree in numerical modelling of nonlinear pulse propagation in semiconductor fibers with the Optoelectronics Research Centre, University of Southampton, Southampton, U.K.

**Shiyu Sun** Shiyu Sun received the B.Eng. degree in Optoelectronics Materials and Devices from Nanjing Tech University, Nanjing, China, in 2016. After that, she received the M. Eng. degree in Optical Engineering from the Huazhong University of Science and Technology, Wuhan, China, in 2019. Since 2019, she has been working toward the Ph. D. degree with the Optoelectronics Research Centre, University of Southampton, Southampton, U.K. Her current research interests are focused on the nonlinearity of the silicon waveguides.

**Thomas W. Hawkins** Thomas W. Hawkins earned the BS, MS, and PhD in Materials Science and Engineering from Clemson University in 1999, 2005, and 2020, respectively. Currently, he is the Optical Fiber Fabrication Laboratory Director and Research Assistant Professor at Clemson where he has published over 90 papers on a wide variety of novel glass, crystalline, semiconductor, polymer, and photonic crystal fibers.

**Ursula J. Gibson** Ursula J. Gibson received the A.B. degree from Dartmouth College, Hanover, NH, USA, and the Ph.D. degree in physics from Cornell University, Ithaca, NY, USA, in 1982. She then held assistant and associate professorships at the University of Arizona's Optical Sciences Center, Tucson, AZ, USA. In 1990, she joined Dartmouth's Thayer School of Engineering. She is currently a Professor of physics with the Norwegian University of Science and Technology, Trondheim, Norway, and holds adjunct positions in applied physics with the KTH Royal Institute of Technology, Stockholm, Sweden, and the Chemistry Department, Dartmouth College. She has more than 100 refereed journal articles, seven book chapters, and three U.S. patents. In 2008, she held a Fulbright Scholarship, working at VTT research labs in Espoo, Finland. She is a Fellow of, and served as the 2019 President of the Optical Society, OSA.

**Periklis Petropoulos** Periklis Petropoulos received the graduate degree from the Department of Electrical Engineering and Information Technology, University of Patras, Patras, Greece, in 1995, the M.Sc. degree in communications engineering from the University of Manchester Institute of Science and Technology, Manchester, U.K., and the Ph.D. degree in optical telecommunications from the Optoelectronics Research Centre (ORC), University of Southampton, Southampton, U.K. He is currently a Professor with the ORC, University of Southampton. His research interests lie in the fields of optical communications, all-optical signal processing and novel fibre and waveguide technologies. He has participated in several European Union and national research projects in the field of optical communications. His research has produced more than 500 papers in technical journals and conference proceedings, including several invited and post-deadline papers in major international conferences, and holds six patents. Dr. Petropoulos has served as a member of the Technical Programme Committees for several international conferences, including the European Conference on Optical Communication (ECOC), the Optical Fiber Communication (OFC) conference, and the European Conference on Lasers and Electro-Optics (CLEO/Europe). He is a Fellow of the Optical Society.

**John Ballato** John Ballato is a professor of materials science and engineering at Clemson University (Clemson, SC USA) where he holds the Sistine Endowed Chair of Optical Fiber. A Fellow of the OSA, IEEE, AAAS, SPIE, and ACerS, Ballato has over 425 publications, 35 US and foreign patents, and is an elected member of the World Academy of Ceramics (limited to < 300 members world-wide) and the US National Academy of Inventors (NAI). His collaborative work on Anderson localizing optical fiber was selected as one of the Top Ten Breakthroughs of 2014 by Physics World (Institute of Physics, IoP).

**Anna C. Peacock** Anna C. Peacock received the B.Sc. and M.Sc. degrees in physics from the University of Auckland, Auckland, New Zealand, in 1999 and 2001, respectively, and the Ph.D. degree from the Optoelectronics Research Centre (ORC), University of Southampton, Southampton, U.K., in 2004. She is a Professor of photonics with the ORC, University of Southampton. In 2007, she received a five-year Royal Academy of Engineering Research Fellowship, following which she established the Nonlinear Semiconductor Photonics Group, where the focus of the research is on the design and development of novel semiconductor waveguides. She is a Fellow of the Optical Society and the Institute of Physics and currently holds a five-year EPSRC research fellowship.